

**Broadband Purcell factor enhancements in photonic-crystal ridge waveguides**

M. Patterson and S. Hughes\*

*Department of Physics, Queen's University, Kingston, Ontario, Canada K7L 3N6*

D. Dalacu and R. L. Williams

*Institute for Microstructural Sciences, National Research Council, Ottawa, Ontario, Canada K1A 0R6*

(Received 12 June 2009; revised manuscript received 31 July 2009; published 11 September 2009)

We introduce the concept and theory for a photonic-crystal ridge waveguide in high index semiconductors that can be used to tailor the single-photon emission of an embedded quantum dot. The design exploits a band structure with a large bandwidth of slow light. By tuning the device geometry, the group velocity of the fundamental waveguide mode and the Purcell factor (enhanced spontaneous emission) can be uniquely controlled. We give reference designs with a Purcell factor of at least 10 and 43 with a large bandwidth of 435 and 51 GHz ( $\sim 1.8$  meV and 0.21 meV), respectively. Applications toward chip-based single-photon emitters are discussed, and a comparison with dispersion-engineered planar photonic-crystal waveguides is also given.

DOI: [10.1103/PhysRevB.80.125307](https://doi.org/10.1103/PhysRevB.80.125307)

PACS number(s): 85.60.-q, 42.70.Qs, 42.50.-p, 42.79.Gn

**I. INTRODUCTION**

Semiconductor chip-based nanostructures that integrate photonic dots and electronic dots offer unprecedented control at the single exciton level, allowing one to nanoengineer efficient single-photon sources for applications in quantum information processing. Early works with semiconductor nanostructures demonstrated the Purcell effect<sup>1</sup> by coupling quantum dots (QDs) to semiconductor microposts.<sup>2-4</sup> More recently, planar photonic crystals (PCs) have been proposed as an efficient single-photon source platform since they exhibit cavity quality factors ( $Q$ 's) as large as  $10^6$  in Si (Refs. 5 and 6) and 700 000 in GaAs (Ref. 7) with small effective mode volumes  $V_{\text{eff}} \sim 0.1 \mu\text{m}^3$ . Planar PCs allow a very rich degree of control of light propagation<sup>8</sup> and photon emission.<sup>9</sup> Single QDs have also been embedded in PC cavities and used to generate single photons<sup>10,11</sup> and demonstrate strong coupling.<sup>12,13</sup> Despite the successes of semiconductor posts and PC cavities, single narrowband cavities are not the ideal platform for single-photon generation applications since it is difficult to extract and transport the photon for further processing and the narrow cavity resonance must be tuned to precisely match the target QD exciton resonance.

To overcome some of the problems of narrowband cavity systems, it has been shown that *open system cavity quantum electrodynamics* (QED) may be exploited to achieve photon emission enhancements by appropriate band-gap engineering of the nanostructured propagation modes.<sup>14-16</sup> In these systems, both fast emission (Purcell effect) and directional emission into the desired channel can be achieved by using the unique properties of periodic waveguides. The regime of slow light mimics the high quality factor of the PC cavities, while the periodic waveguide mode has a significantly reduced effective mode volume. Related experiments on PC waveguides have been performed in Refs. 17 and 18. Although these experiments demonstrate that waveguide systems are potentially useful for single-photon applications, hitherto, there has been little guidance from theoretical works in terms of optimal waveguide parameters.

The general requirements for a single-photon source include emission of only a single photon, fast emission to pre-

vent the detrimental effects of decoherence and photon emission into a controllable output channel. Single emission can be achieved using a single QD since Coulomb interactions and structural asymmetries (anisotropic exchange splitting) break the degeneracy between single and multiple exciton transitions. Fast emission and emission into the desired channel can be achieved through the combination of a large Purcell effect and a large  $\beta$  factor, where the latter gives a measure of the photon emission into a desired output channel. To achieve such a rich degree of control of the single photons, we will need optimized single-photon sources and high performance waveguides.

Waveguides in PC crystals support quasi-one-dimensional Bloch modes (the mode profile is three dimensional but there is periodicity only along one dimension) that can have complex dispersion relations. In particular, it is common to find a waveguide mode with a slow-light propagation region near the band edge. Such structures have been explored extensively as optical delay lines<sup>8</sup> and have been optimized<sup>19-21</sup> for linear-dispersion slow light. Their germane property is that a slow-light waveguide enhances the spontaneous emission and, as a waveguide, is ideal for transporting the emitted single photon. The simplest waveguide is formed by omitting a single row of holes in a triangular lattice (the W1 waveguide) and has been used to experimentally demonstrate Purcell factor enhancements.<sup>18</sup>

In this work, we propose a carefully optimized PC waveguide design that affords both a large bandwidth for slow-light propagation and enhanced spontaneous emission. The design is tailored to be fully compatible with experimental site-selective growth techniques for self-assembled InAs/InP QDs, with the intent that the PC waveguide can be used to efficiently collect photons from single QDs and possibly to pass them on to other dots that are spatially remote. In contrast to previous dispersion engineering approaches, we focus not on low-dispersion slow light, but on achieving a desired practical minimum Purcell factor (driven by a local minimum group index) over a broad frequency range. To this end, we propose a PC slab waveguide design in which the slab is augmented with a trapezoidal or triangular cross-section ridge, as shown schematically in Fig. 1(a) and in the

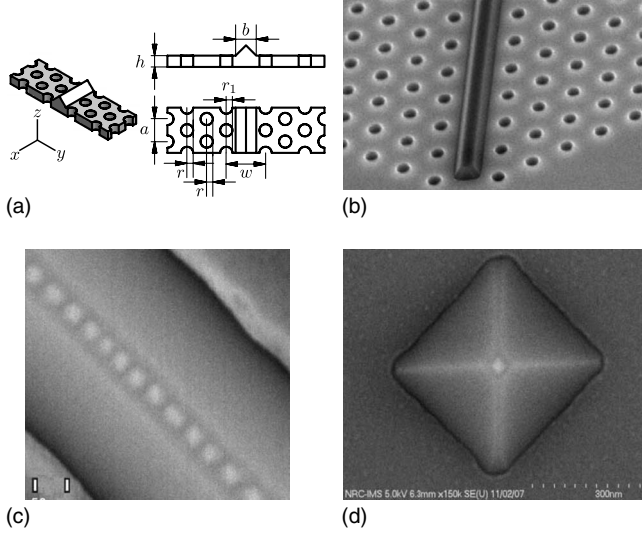


FIG. 1. (a) Schematic diagram of two periods of the waveguide structure showing the parameters that describe the device geometry. (b) Scanning electron micrograph (SEM) of a typical structure. (c) SEM of quantum dot nucleation within the waveguide. (d) Quantum dot nucleation on a pyramidal InP template which could be planarized by overgrowing the pyramid and substrate to form a slab with an embedded deterministically placed QD.

scanning electron micrograph of Fig. 1(b). High quality ridges of this type, with extremely smooth {110} or {111} side walls, can be grown using selective area epitaxy and the ridge itself can be used to control the nucleation site of InAs/InP quantum dots, as shown in Fig. 1(c). Alternatively, single InAs/InP QDs can be grown on pyramidal InP templates with {110} side walls [see Fig. 1(d)], and planarized by overgrowing the entire structure with InP to produce the slab necessary for PC fabrication. In this case, a second growth step would be used to define the guiding ridge structure, with the advantage that the location of the QD can be fully controlled with respect to the apex of the ridge. Full details of the processing for these site-selective QDs structures can be found in Ref. 22.

In Sec. II, we introduce the general theory describing enhanced spontaneous emission in a periodic waveguide structure. In Sec. III, the basic structure and material parameters are presented, where we calculate the waveguide band structure, Bloch modes, and Purcell factor as a function of position. In Sec. IV, we optimize the structural parameters to achieve a desired Purcell factor over a specific bandwidth; we also discuss the single-photon  $\beta$  factors and effective mode volumes, and present a summary of our design in a table of parameters. In Sec. V, we carry out our calculations for another broadband slow-light planar PC waveguide used in Ref. 20. Our conclusions are given in Sec. VI.

## II. THEORY

The radiative emission rate of a dipole or QD exciton is not an intrinsic property of the emitter but can be altered by the local electromagnetic environment, namely, through the Purcell effect.<sup>1</sup> The radiative emission rate  $\Gamma$  (frequently

termed the *Einstein A* coefficient) is controlled by the local density of states (LDOS), proportional to  $\text{Im}[\vec{\mathbf{G}}(\mathbf{r}, \mathbf{r}; \omega)]$ , where  $\vec{\mathbf{G}}(\mathbf{r}, \mathbf{r}'; \omega)$  is the photon Green's function, obtained from a dipole solution to the full Maxwell equations. Specifically, the Green's function is defined from

$$\left[ \nabla \times \nabla \times - \frac{\omega^2}{c^2} \epsilon(\mathbf{r}) \right] \vec{\mathbf{G}}(\mathbf{r}, \mathbf{r}'; \omega) = \frac{\omega^2}{c^2} \vec{\mathbf{1}} \delta(\mathbf{r} - \mathbf{r}'), \quad (1)$$

where  $\vec{\mathbf{1}}$  is the unit dyadic and  $\epsilon(\mathbf{r})$  is the dielectric constant for the material. For a homogeneous dielectric,

$$\text{Im}[\vec{\mathbf{G}}_0(\mathbf{r}, \mathbf{r}; \omega)] = \frac{\omega^3 \sqrt{\epsilon}}{6\pi c^3} \vec{\mathbf{1}}. \quad (2)$$

From these definitions, it follows that

$$\Gamma(\mathbf{r}, \omega) = \frac{2\mathbf{d} \cdot \text{Im}[\vec{\mathbf{G}}(\mathbf{r}, \mathbf{r}; \omega)] \cdot \mathbf{d}}{\hbar \epsilon_0}, \quad (3)$$

where  $\mathbf{d}$  is the dipole moment of the emitter.

In a PC waveguide, we can decompose the Green's function as  $\vec{\mathbf{G}}(\mathbf{r}, \mathbf{r}'; \omega) = \vec{\mathbf{G}}_{\text{bound}}(\mathbf{r}, \mathbf{r}'; \omega) + \vec{\mathbf{G}}_{\text{other}}(\mathbf{r}, \mathbf{r}'; \omega)$ , where  $\vec{\mathbf{G}}_{\text{bound}}(\mathbf{r}, \mathbf{r}'; \omega)$  is the contribution due only to the bound waveguide mode. This can be written analytically in terms of the properties of the mode as<sup>14</sup>

$$\begin{aligned} \vec{\mathbf{G}}_{\text{bound}}(\mathbf{r}, \mathbf{r}'; \omega) = & i \frac{a\omega}{2v_g} [\mathbf{e}_k(\mathbf{r}) \otimes \mathbf{e}_k^*(\mathbf{r}') e^{ik(x-x')} \Theta(x-x') \\ & + \mathbf{e}_k^*(\mathbf{r}) \otimes \mathbf{e}_k(\mathbf{r}') e^{ik(x'-x)} \Theta(x'-x)], \end{aligned} \quad (4)$$

where  $a$  is the periodic pitch of the PC lattice,  $v_g$  (treated as positive) is the waveguide group velocity,  $\mathbf{e}_k(\mathbf{r})$  is the waveguide Bloch mode electric field with wave vector  $k$  normalized by  $\int_{\text{unit cell}} d\mathbf{r} \epsilon(\mathbf{r}) |\mathbf{e}_k(\mathbf{r})|^2 = 1$ ,  $\otimes$  is an outer (tensor) product, and  $\Theta(x)$  is the Heaviside step function equal to 1 if  $x > 0$  and 0 if  $x < 0$ .

The Purcell factor is defined as the ratio of the radiative emission rate into the mode of interest of the inhomogeneous structure  $\Gamma_w$ , to the radiative emission rate in a corresponding homogeneous dielectric  $\Gamma_0$ . The Purcell factor is thus a measure of the enhancement of the *projected* LDOS and the spontaneous emission rate. To apply the Purcell effect as a direct measure of the spontaneous emission rate, one needs to be in the weak to intermediate coupling regimes, so that the QD exciton is not strongly coupled to the photonic modes in the surrounding material. For a dipole placed in a PC waveguide, the component of the LDOS due to the waveguide mode can be written analytically in terms of properties of the mode. Consequently, the Purcell factor for a PC waveguide mode is<sup>14,15</sup>

$$\begin{aligned} F_w(\mathbf{r}_d, \omega) = \frac{\Gamma_w}{\Gamma_0} = & \frac{\mathbf{d} \cdot \text{Im}[\vec{\mathbf{G}}_{\text{bound}}(\mathbf{r}, \mathbf{r}; \omega)] \cdot \mathbf{d}}{\mathbf{d} \cdot \text{Im}[\vec{\mathbf{G}}_0(\mathbf{r}, \mathbf{r}; \omega)] \cdot \mathbf{d}} \\ = & \frac{3\pi c^3 a}{v_g(\omega) \sqrt{\epsilon(\mathbf{r}_d)} \omega^2} |\mathbf{e}_k(\mathbf{r}_d) \cdot \hat{\mathbf{n}}|^2, \end{aligned} \quad (5)$$

where  $\mathbf{r}_d$  is the dipole position, and  $\hat{\mathbf{n}}$  is a unit vector parallel to the dipole orientation.

The Purcell factor captures emission into the waveguide mode; however there will also be undesirable emission into other modes of the system such as pure radiation modes which enable light to escape from the PC slab. For single-photon emission applications, it is not enough for a structure to have a large Purcell factor; it must also emit the majority of its photons into the desired waveguide mode. In this regard, the  $\beta$  factor expresses the probability that an emitted photon will be emitted into a target waveguide mode:<sup>15</sup>

$$\beta = \frac{\Gamma_w}{\Gamma_w + \Gamma_{rad} + \dots} = \frac{F_w}{F_w + \Gamma_{rad}/\Gamma_0 + \dots}, \quad (6)$$

where the “...” indicates any other emission channels such as a second waveguide mode or through nonradiative decay. The  $\beta$  factor can be influenced in a number of ways. If the radiative decay rate is reduced by placing the dot in a PC material, or even a slab,  $\beta$  will increase. However in this case, placing the dot in the ridge leads to a radiation LDOS similar to a homogeneous structure. Here we exploit the slow group velocity which increases the Purcell factor and consequently increases  $\beta$ . There have been other approaches to optimizing  $\beta$  without the Purcell effect, such as those reported in Ref. 16.

### III. BASIC STRUCTURE AND PROPERTIES

We propose a hybrid structure between a PC slab waveguide and a triangular ridge waveguide as shown schematically in Fig. 1(a) (with the same coordinate system used in this discussion). The ridge is formed from the natural {110} surfaces of InP and so will be atomically smooth. The vertical asymmetry creates an anticrossing in the band structure, which leads to a band of slow light that can enhance spontaneous emission. Other advantages of this structure are that it may be more resilient to slow-light scattering losses,<sup>23-25</sup> due to the ideally smooth ridge walls. It may also be possible to have only a short section of the waveguide use PC confinement near the dot and use a traditional strip waveguide to transport the photon over long distances.

We will first examine the main properties of a baseline structure and subsequently, in the next section, optimize the design. The calculations are performed assuming fabrication from InP ( $n=3.17$ ) and a periodicity (hole to hole pitch) of  $a=420$  nm. The ridge is surrounded by PC cladding composed of air holes ( $r=0.27a$ ) arranged in a triangular lattice. The PC has a photonic band gap for pseudotransverse electric (TE) modes over the frequency range of interest. Pseudo-TE modes are analogous to the true TE modes of a two-dimensional waveguide in that the electric field is generally perpendicular to the propagation direction; however the longitudinal ( $x$ ) component is not identically zero in places due to the lack of perfect translational invariance in  $x$ . The waveguide mode at the point of interest has the electric field polarized along the  $y$  direction for optimal coupling to a QD exciton mode and so we will calculate the Purcell factor for a  $y$ -polarized dipole.

The waveguide dispersion and Bloch modes are calculated with a frequency-domain plane-wave expansion technique using a freely available software package.<sup>26</sup> The band

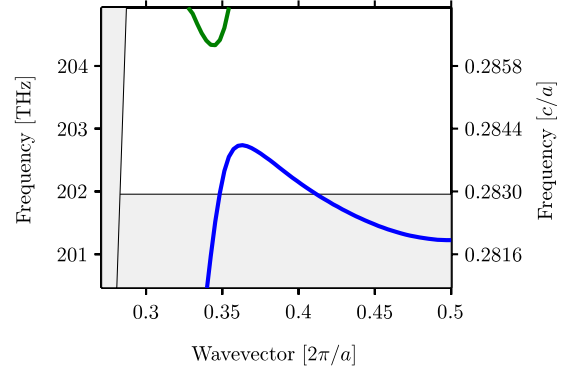


FIG. 2. (Color online) Band structure for the baseline structure. The primary waveguide mode is plotted in blue. The gray region at the bottom of the plot indicates frequencies outside the photonic band gap. The gray region to the left represents the continuum of radiation modes above the light line.

structure is shown in Fig. 2 with the primary waveguide mode plotted in blue. The waveguide mode has an anticrossing at  $k \approx 0.35 \times 2\pi/a$ , where the group velocity,  $v_g = d\omega/dk$ , goes to 0. The group velocity also goes to zero at the band edge ( $k = 0.5 \times 2\pi/a$ ). Between these points, there is a large bandwidth region with a low group velocity and a high Purcell factor. The gray region at the bottom of the figure is below the band gap of the surrounding PC and the gray region to the left represents the continuum of radiation modes above the light line. The presence of the ridge allows the mode to expand slightly, leading to a lower band-edge frequency than a standard W1 waveguide and the band-edge dips outside of the photonic band gap. The optimized designs will lie inside the photonic band gap; however this mode can still be well confined by dielectric contrast as shown by simulations and experimental data with past devices.<sup>27</sup> In addition, the presence of the ridge will help ensure a true bound mode below the light line, even for frequencies outside the photonic band gap. The primary purpose of the PC is to introduce periodicity which creates the slow-light band.

The Purcell factor has a strong spatial dependence due to its relation to the Bloch mode electric field. The electric field profile for the mode near the band edge is shown in Fig. 3

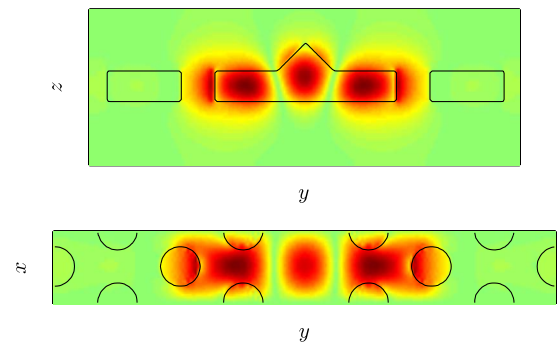


FIG. 3. (Color online) Absolute value of the electric field  $y$  component for the fundamental waveguide mode near the band edge. The top plot is a plane of constant  $x$  that passes through the field antinodes. The bottom plot is a plane of constant  $z$  that pass through the center of the PC slab.

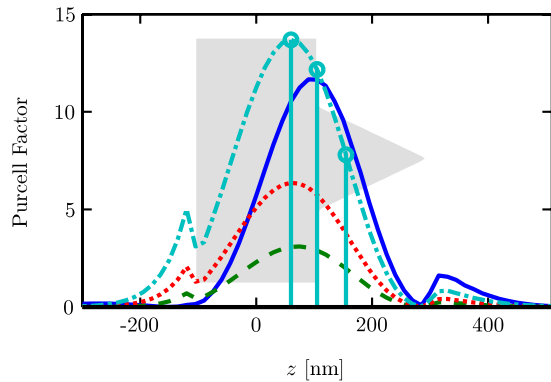


FIG. 4. (Color online) Purcell factor as a function of height on a line through the center of a unit cell. The gray watermark schematically shows the structure and the different lines correspond to different wave vectors:  $0.367$  (blue, solid),  $0.400$  (green, dashed),  $0.434$  (red, dotted), and  $0.467 \times 2\pi/a$  (cyan, dot-dashed). The cyan stems mark the three dipole heights ( $z$  values) of interest from left to right: at the antinode, at the height of the slab level, and  $50$  nm above the slab level.

and has three antinodes, with one under the ridge and two in the slab interacting with the PC. For optimal coupling, we desire to place the QD as close to an antinode as possible. For ease of fabrication, we target the central antinode. The Purcell factor is shown in Fig. 4 as a function of height ( $z$ ) for a QD placed on a line passing through the antinode. To complicate the design process, the antinode position moves slightly as a function of wave vector, starting above the flat surface level at  $k=0.367 \times 2\pi/a$  (blue, solid) and sinking into the slab as the wave vector increases (green, dashed; then red, dotted; then cyan, dot-dashed). The change in magnitude of the Purcell factor is caused mostly by a change in the group velocity as a function of wave vector. Since there is not always complete experimental control over the QD position, we will present results for three possible  $z$  values. The bottom point is at the antinode (at the band edge) and couples most strongly to the field. This position is recalculated each time the structure is altered. The middle position is at the level of the surrounding slab. The top point is  $50$  nm above the level of the surrounding slab. These three positions are marked in Fig. 4.

The Purcell factor is plotted as a function of frequency in Fig. 5 for the three dot positions in the nominal structure. The downward sloping portion of the band in Fig. 2 corresponds to the region of high Purcell factor bounded on either side by LDOS divergences. The dashed portion of the curve corresponds to the upward sloping portion of the band and is shown for completeness but does not have a pronounced Purcell enhancement. At the mode edge, the Purcell factor theoretically diverges (at least for perfect structures in the absence of fabrication imperfections), when  $v_g=0$ , and so it is difficult to compare results for different structures. Therefore, we propose to describe structures with two well-defined practical quantities that can be measured: the minimum Purcell factor and the bandwidth of the slow-light region. The bandwidth is defined as the frequency difference between the band edge and the frequency maximum, i.e., the bandwidth between the two divergences in the Purcell factor plot. This

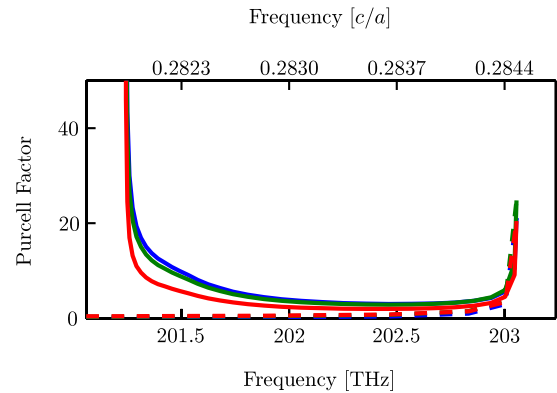


FIG. 5. (Color online) Purcell factor (y component) for the baseline structure at three different positions, the antinode (blue, top solid curve), the slab level (green, middle solid curve), and  $50$  nm above the level (red, bottom solid curve). The dashed portion of the curve is shown for completeness and is for emission into the portion of the mode before the anticrossing.

slightly overestimates the useful bandwidth since we are not interested in operating the device near the frequency maximum due to the poorer mode confinement and potentially higher losses. By operating close to the band edge, Purcell factors greatly exceeding the minimum Purcell factor can be achieved. Although not exact, the computed bandwidth and minimum Purcell factor capture the essence of the desired operational characteristics. For the baseline structure, the minimum Purcell factors are  $3.02$ ,  $2.87$ , and  $1.96$  for the three QD positions (antinode, level, and  $50$  nm above the level). The minimum group index (corresponding to the minimum Purcell factor) is  $28$ . The bandwidth of this region is  $0.00254c/a$  or  $1.8$  THz ( $\sim 7.4$  meV). It should be noted that this is significantly larger than the bandwidth of a typical PC cavity mode (on the order of a few GHz).

#### IV. STRUCTURE OPTIMIZATION AND TWO EXAMPLE DESIGNS

Next we investigate the sensitivity of the structure properties to many of the structural parameters shown in Fig. 1(a). We provide general remarks on each of the parameters and present two reference designs for enhanced spontaneous emission. Any structural changes add or remove dielectric and the most obvious result is a frequency shift of the mode. This is, in fact, a distraction since the structure can be tuned to the frequency of interest by scaling the periodicity  $a$ . For this reason, frequencies are given in normalized units of  $c/a$  as well as in THz for a reference pitch,  $a=420$  nm. It is the interaction of the waveguide mode with the periodic PC cladding that creates the interesting slow-light behavior, and tuning the structure is achieved by the alteration of this coupling and the resultant changes in the slow-light region. As the structure is altered, the frequency maximum, initially at  $k=0.35 \times 2\pi/a$ , can shift to higher (lower) wave vectors, leading to a decrease (increase) in the slow-light bandwidth but an increase (decrease) in the group index. Figure 6 illustrates this phenomenon for one of the structure parameters.

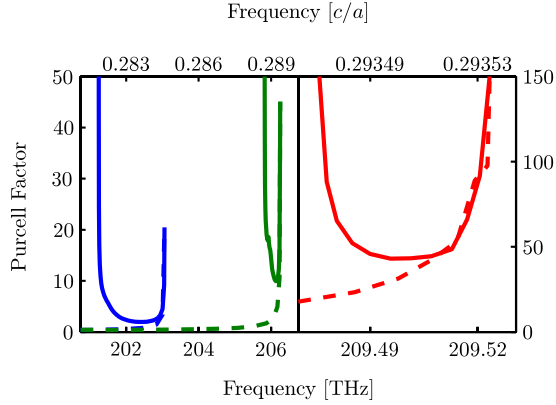


FIG. 6. (Color online) Purcell factor as a function of frequency for a quantum dot 50 nm above the level of the PC slab. The three curves are for three different values of  $w$ :  $\sqrt{3}a$  (blue, left curve),  $(\sqrt{3}-0.12)a$  (green, middle curve), and  $(\sqrt{3}-0.20)a$  (red, right curve, right scale). The dashed portion of the curve is shown for completeness and is for emission into the portion of the mode before the anticrossing. The apparent dislocation at 209.52 THz is due to this section of the mode being poorly resolved in the simulations; we are interested in emission in the low-frequency part of the spectrum, near the band edge.

The group index and bandwidth are closely linked and their product remains relatively constant.

We examined the slab thickness,  $h$ , dependence of the modes over the range  $0.3-1.0a$ . Although there is a variation in the group velocity with varying slab thickness, for small changes in thickness, the dominant effect is a shift in the antinode location. Thin slabs force the antinode up into the ridge. For thick slabs (above  $0.7a$ ), the bottom two antinodes merge and the mode has two antinodes stacked vertically. Since the slow-light propagation is due to the interaction of the mode with the periodic dielectric, both very thin and very thick slabs are counter productive as they concentrate the mode into the central core and decrease its coupling to the PC cladding. A thickness in the range  $0.4-0.6a$  is found to be optimal, with thicker slabs giving slower propagation. Thus, we use  $h=0.5a$  for our design. If a fabrication process is tuned for a fixed thickness, this is not problematic, provided  $a$  is chosen so the fixed thickness is in the  $0.4-0.6a$  range.

The triangular ridge creates the unusual band structure for this device, but the device properties are relatively insensitive to the precise width of the ridge,  $b$ , and there is little to be gained by tweaking this value. The group velocity is relatively constant as the width varies from  $0.85$  to  $1.1a$ . At larger widths, the group index does increase but the base of the ridge is almost overlapping the first row of holes. The

dominant effect in changing the width is a frequency shift and a slight shift in the position of the central antinode. Therefore,  $b=0.91a$  is used since it allows room for tuning the structure with the waveguide width.

The nominal width of the waveguide measured between the centers of the flanking holes is  $w=\sqrt{3}a$ . We investigated the effect of making the waveguide slightly larger by shifting the PC perpendicular to the propagation direction. Increasing  $w$  leads to an increase in bandwidth at the cost of a decreasing group index and Purcell factor, and is not recommended. The structure is very sensitive to small decreases in  $w$ , which cause the Purcell factor to increase rapidly. Tuning  $w$  presents one of the best opportunities for tuning the slow-light bandwidth of these structures. Similar tuning has been performed in PC waveguides without the ridge.<sup>20</sup> The Purcell factor for a dot 50 nm above the level of the PC slab is shown in Fig. 6 for select values of  $w$ . The frequency shift of the band is clearly visible as is the tradeoff between bandwidth and group index (which is proportional to the Purcell factor).

The radius of the holes closest to the waveguide,  $r_1$ , can be varied with the radius of the other rows of holes,  $r$ , unchanged. Similar optimization has been done for standard PC waveguides in Ref. 19. Increasing  $r_1$  has a similar effect to decreasing  $w$ . As the hole radius is increased, the band shifts to higher frequencies and flattens. The bandwidth of the slow-light region decreases, but the group index and Purcell factor increase. In general, the position of the hole center is easier to control than its radius and so we use  $w$  to optimize the structure and leave all holes with identical radii.

Based on this work, we propose two structures of interest to be selected, depending on the application. They are  $w=(\sqrt{3}-0.12)a$  and  $w=(\sqrt{3}-0.20)a$ . The other parameters are  $r=0.27a$ ,  $b=0.91a$ , and  $h=0.5a$ , and  $a=420$  nm. These parameters provide a good trade off between Purcell factor enhancement and bandwidth. These parameters yield Purcell factors of 10 and 43, respectively, for a dot 50 nm above the level. The bandwidths are 435 GHz ( $\sim 1.8$  meV) and 51 GHz ( $\sim 0.21$  meV). If the dots were optimally coupled to the antinode, the Purcell factors could be increased to 14 and 67. A summary of some figures of merit for these structures is given in Table I. A detailed summary of the data for the optimization with respect to  $w$  is given in Fig. 7, so that one can optimize for different Purcell factors or bandwidths.

Using a radiative emission rate equal to that in a homogeneous background (determined from finite-difference time-domain simulation),<sup>28</sup> neglecting the influence of nonradiative decay (appropriate for low temperature, e.g.,  $T=4$  K), and neglecting the small contribution from other modes (as shown in, e.g., Fig. 5, emission into the half of the mode before the frequency maximum is minimal), we calculate  $\beta$

TABLE I. Summary of the properties of the recommended designs.

$w$ ( $a$ )	Purcell factor at 50 nm	Purcell factor at antinode	Minimum group index	Bandwidth (GHz)	$\beta$ (%)	Pseudo- $Q$	$V_{\text{eff}}$ ( $\mu\text{m}^3$ )
$\sqrt{3}-0.12$	10	14	104	435	91	3 000	0.048
$\sqrt{3}-0.20$	43	67	461	51	98	26 000	0.045

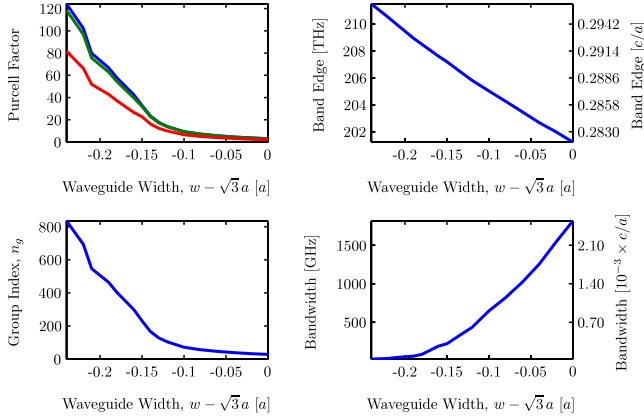


FIG. 7. (Color online) Properties of the slow-light region under variations in the waveguide width,  $w$ . The top left plot shows the minimum Purcell factor for the three dot heights: antinode (blue, top curve), level (green, middle curve), and 50 nm above the level (red, bottom curve). The top right plot shows the shift of the band-edge frequency. The bottom left plot show the increase in the group index with decreasing  $w$ . Finally, the bottom right plot shows the associated bandwidth tradeoff.

factors of 91% and 98%, respectively. The  $\beta$  factor is the probability for an emitted photon to end up in the waveguide mode traveling in either of the two directions. By closing one end of the waveguide with a PC mirror (e.g., by changing the pitch of the PC cladding or adding additional holes), unidirectional output can be achieved, although care must be taken to place the emitter at a point where the emitted forward wave and reflected wave interfere constructively.<sup>29</sup> Thus these designs allow for almost all the emitted light to be collected into a well-controlled channel.

It is interesting to compare the properties of this open waveguide system with a closed PC cavity. We can provide a rough comparison of the spectral properties by constructing a pseudo- $Q$  for the waveguide structures. The traditional definition of  $Q$ , the quality factor, for a cavity is  $Q=2\pi f/\Gamma_c$ , where  $f$  is the mode frequency and  $\Gamma_c$  is the cavity decay rate or line width. Using the slow-light bandwidth in place of  $\Gamma_c$ , we can get a comparison of how the bandwidth of our waveguide structure compares with a cavity structure. We can also calculate an effective mode volume for the waveguide as  $V_{\text{eff}}=(\epsilon(\mathbf{r}_a)|\mathbf{e}_k(\mathbf{r}_a)|^2)^{-1}$  evaluated at the antinode position,  $\mathbf{r}_a$ , with the pitch  $a$  taken as the third dimension and with the normalization  $\int_{\text{unit cell}} \epsilon(\mathbf{r})|\mathbf{e}_k(\mathbf{r})|^2 d\mathbf{r}=1$ . The pseudo- $Q$ 's and effective mode volumes for the two proposed structures are given in Table I.

**V. COMPARISON WITH OTHER DISPERSION-ENGINEERED SLOW-LIGHT WAVEGUIDES**

Our general design approach is not restricted to ridge waveguide PCs, and can be applied to any periodic dielectric system. Thus, it is instructive to compare the properties of this waveguide with other dispersion-engineered structures, which have previously been optimized for broadband and slow-light applications. For example, Li *et al.*<sup>20</sup> report on a slow-light waveguide formed from a W1 (missing row of holes) waveguide by shifting the first rows of holes a dis-

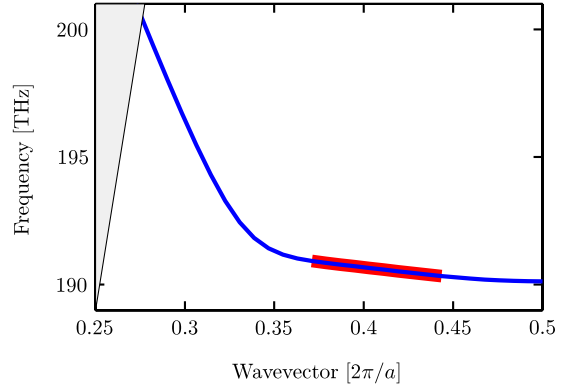


FIG. 8. (Color online) Dispersion relation for Li's  $s_1=-0.1$ ,  $s_2=0.085a$  engineered waveguide mode (Ref. 20). The mode has a region with a near-constant group velocity  $v_g=c/90$  (highlighted in red). The gray region to the left represents the continuum of radiation modes above the light line.

tance  $s_1$  toward the waveguide core and shifting the second row of holes a distance  $s_2$  ( $s_1$  is usually negative). We have reproduced simulations for their proposed  $s_1=-0.1$ ,  $s_2=0.085a$ , and  $a=414$  nm structure, hereafter referred to as Li's structure. The dispersion relation for the fundamental waveguide mode is shown in Fig. 8. They optimized the design to produce a band of relatively low-dispersion slow light with  $n_g=90$  (red highlighted region of the band structure), and based on the findings above, this structure will also exhibit a broadband Purcell enhancement. This structure has similar properties to our  $w=(\sqrt{3}-0.12)a$  structure, which has a local minimum group index (in the slow light region) of 104.

Using the computed band structure and modes, we directly compare the Purcell factor for our and Li's structures in Fig. 9. We also compare both structures with an unoptimized W1 waveguide. The Purcell factor is evaluated at the

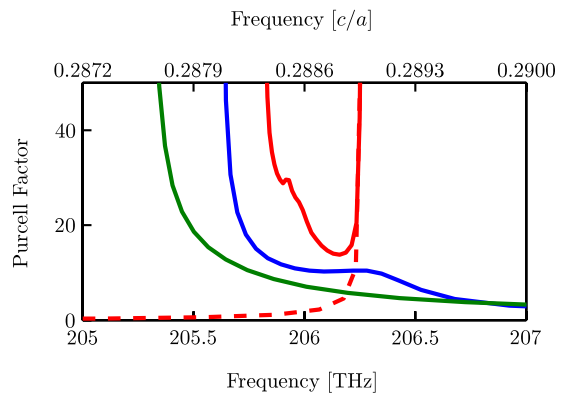


FIG. 9. (Color online) Comparison of the Purcell factor between Li's  $s_1=-0.1$ ,  $s_2=0.085a$ ,  $n_g=90$  design (blue, middle solid curve), an unoptimized W1 waveguide (green, bottom solid curve), and the  $w=(\sqrt{3}-0.12)a$  design (red, top solid curve). A frequency shift has been applied to Li's data and the W1 to superimpose them with our structure (cf. Fig. 8). All Purcell factors are calculated at the antinode. The dashed portion of the curve is shown for completeness and is for emission into the portion of the mode before the anticrossing.

antinode in both cases, yielding values of 14 for our design and 10 for Li's. Li's structure has a slightly larger bandwidth as shown in the figure. We can also calculate the group-index normalized-bandwidth product  $n_g \times \Delta f/f$  for quantitative comparison. Our designs yield figures of merit of 0.21 and 0.11 for  $w=(\sqrt{3}-0.12)a$  and  $(\sqrt{3}-0.2)a$ , respectively. Li's design has a figure of merit of 0.3 but this was precisely the quantity that they sought to optimize. Both engineered structures outperform the W1 by having a bandwidth where the group velocity and Purcell factor can be tuned to a desired value.

These numbers of course must be used in conjunction with challenges of embedding a single QD at precise spatial locations. Nevertheless, we have presented realistic and conservative numbers for the proposed waveguide structures. Thus, we believe that this general class of dispersion-engineered slow-light waveguides shows significant promise for single-photon emission applications, and related experiments are already coming to the fore.<sup>18</sup> Future work should look at incorporating a coupler, and assessing the role of finite-size effects, such as those reported in Ref. 29.

## VI. CONCLUSIONS

We have introduced the idea of "a dispersion-engineered PC" waveguide formed by adding a ridge formed by natural

crystallographic facets on top of a standard W1-like waveguide for use in single-photon emission applications. The motivation of using such structures stems from the ability of performing site-selective positioning of single QDs. The vertical asymmetry naturally creates a broadband region of slow-light propagation that is ideal for enhancing emission from embedded QDs and channeling the light into the waveguide. We provide two reference designs with Purcell factors of at least 10 and 43 over bandwidths of 435 and 51 GHz ( $\sim 1.8$  and  $0.21$  meV), respectively. These waveguides are competitive with other recent dispersion-engineered structures and could be used to produce high efficiency single-photon sources for application in quantum information processing.

## ACKNOWLEDGMENTS

This work was supported by the National Sciences and Engineering Research Council of Canada, the Canadian Foundation for Innovation, and QuantumWorks. We are grateful to V. S. C. Manga Rao and T. Krauss for useful discussions.

\*shughes@physics.queensu.ca

<sup>1</sup>E. M. Purcell, Phys. Rev. **69**, 681 (1946), see [http://prola.aps.org/pageif/PR/v69/i11-12/p674\\_2/p681](http://prola.aps.org/pageif/PR/v69/i11-12/p674_2/p681)

<sup>2</sup>E. Moreau, I. Robert, J. M. Gérard, I. Abram, L. Manin, and V. Thierry-Mieg, Appl. Phys. Lett. **79**, 2865 (2001).

<sup>3</sup>C. Santori, D. Fattal, J. Vuković, G. S. Solomon, and Y. Yamamoto, Nature (London) **419**, 594 (2002).

<sup>4</sup>M. Pelton, C. Santori, J. Vučković, B. Zhang, G. S. Solomon, J. Plant, and Y. Yamamoto, Phys. Rev. Lett. **89**, 233602 (2002).

<sup>5</sup>Y. Akahane, T. Asano, B.-S. Song, and S. Noda, Nature (London) **425**, 944 (2003).

<sup>6</sup>E. Kuramochi, M. Notomi, S. Mitsugi, A. Shinya, T. Tanabe, and T. Watanabe, Appl. Phys. Lett. **88**, 041112 (2006).

<sup>7</sup>S. Combrié, A. De Rossi, Q.-V. Tran, and H. Benisty, Opt. Lett. **33**, 1908 (2008).

<sup>8</sup>T. Baba, Nat. Photonics **2**, 465 (2008).

<sup>9</sup>S. Noda, M. Fujita, and T. Asano, Nat. Photonics **1**, 449 (2007).

<sup>10</sup>D. Englund, D. Fattal, E. Waks, G. Solomon, B. Zhang, T. Nakaoka, Y. Arakawa, Y. Yamamoto, and J. Vučković, Phys. Rev. Lett. **95**, 013904 (2005).

<sup>11</sup>W.-H. Chang, W.-Y. Chen, H.-S. Chang, T.-P. Hsieh, J.-I. Chyi, and T.-M. Hsu, Phys. Rev. Lett. **96**, 117401 (2006).

<sup>12</sup>T. Yoshie, A. Scherer, J. Hendrickson, G. Khitrova, H. M. Gibbs, G. Rupper, C. Ell, O. B. Shchekin, and D. G. Deppe, Nature (London) **432**, 200 (2004).

<sup>13</sup>K. Hennessy, A. Badolato, M. Winger, D. Gerace, M. Atature, S. Gulde, S. Falt, E. L. Hu, and A. Imamoglu, Nature (London) **445**, 896 (2007).

<sup>14</sup>S. Hughes, Opt. Lett. **29**, 2659 (2004).

<sup>15</sup>V. S. C. Manga Rao and S. Hughes, Phys. Rev. B **75**, 205437 (2007).

<sup>16</sup>G. Lecamp, P. Lalanne, and J. P. Hugonin, Phys. Rev. Lett. **99**, 023902 (2007).

<sup>17</sup>E. Viasnoff-Schwoob, C. Weisbuch, H. Benisty, S. Olivier, S. Varoutsis, I. Robert-Philip, R. Houdré, and C. J. M. Smith, Phys. Rev. Lett. **95**, 183901 (2005).

<sup>18</sup>T. Lund-Hansen, S. Stobbe, B. Julsgaard, H. Thyrrstrup, T. Sunner, M. Kamp, A. Forchel, and P. Lodahl, Phys. Rev. Lett. **101**, 113903 (2008).

<sup>19</sup>S. Kubo, D. Mori, and T. Baba, Opt. Lett. **32**, 2981 (2007).

<sup>20</sup>J. Li, T. P. White, L. O'Faolain, A. Gomez-Iglesias, and T. F. Krauss, Opt. Express **16**, 6227 (2008).

<sup>21</sup>Y. Hamachi, S. Kubo, and T. Baba, Opt. Lett. **34**, 1072 (2009).

<sup>22</sup>P. J. Poole, G. C. Aers, A. Kam, D. Dalacu, S. Studenikin, and R. L. Williams, J. Cryst. Growth **310**, 1069 (2008).

<sup>23</sup>S. Hughes, L. Ramunno, J. F. Young, and J. E. Sipe, Phys. Rev. Lett. **94**, 033903 (2005).

<sup>24</sup>D. Gerace and L. C. Andreani, Opt. Lett. **29**, 1897 (2004).

<sup>25</sup>M. L. Povinelli, S. G. Johnson, E. Lidorikis, J. D. Joannopoulos, and M. Soljacic, Appl. Phys. Lett. **84**, 3639 (2004).

<sup>26</sup>S. G. Johnson and J. D. Joannopoulos, Opt. Express **8**, 173 (2001).

<sup>27</sup>E. Kuramochi, M. Notomi, S. Hughes, A. Shinya, T. Watanabe, and L. Ramunno, Phys. Rev. B **72**, 161318(R) (2005).

<sup>28</sup>We use FDTD Solutions from Lumerical Solutions, Inc., see <http://www.lumerical.com>

<sup>29</sup>V. S. C. Manga Rao and S. Hughes, Phys. Rev. Lett. **99**, 193901 (2007).